

# Colloidal Silica Rods: Material Properties and Fluorescent Labeling

Anke Kuijk,\* Arnout Imhof, Margriet H. W. Verkuijlen, Thijs H. Besseling, Ernst R. H. van Eck, and Alfons van Blaaderen\*

In this paper, the characterization and fluorescent labeling of silica rods are reported. These rods are synthesized following a recently reported method. Material properties of the silica rods measured with NMR, elemental analysis, TGA, and porosimetry are compared with those of well-established Stöber silica spheres. Additionally, silica rods are made suitable for quantitative real-space studies by confocal microscopy. Several methods of fluorescent labeling to prepare rods with different fluorescent patterning, ranging from uniform fluorescence levels to gradients from one rod-end to the other, and even patterns of several colors are presented and discussed.

## 1. Introduction

Recently, we developed a new colloidal model system that allows for real-space 3D studies of rod-like systems on the single particle level.<sup>[1]</sup> This system, which consists of rod-like silica particles, forms an interesting addition to the existing systems of silica colloids, since it does not consist of spheres, but is shape-anisotropic. The particles are monodisperse enough that they form liquid crystalline phases, such as smectic phases.<sup>[2]</sup> While monodisperse silica spheres made from alkoxy silanes have become a popular model system in colloid science and the properties of these kinds of particles have been studied since their preparation was first described by Stöber et al.<sup>[3]</sup> in 1968, little is known about silica rods made from alkoxy silanes. Yet, it is important to have information about the chemical composition and physical properties of the rods when they are used as a model system. Therefore, we studied the material properties of the rods and compared them to those of spherical Stöber silica.

Furthermore, we examined methods to label silica rods with a fluorescent dye, which is required to use them in fluorescence confocal microscopy studies. Confocal microscopy is a

technique that is frequently used in colloid science to obtain quantitative information in 3D and real space about the structure and dynamics of colloidal systems with single particle resolution.<sup>[4–6]</sup> In recent years, this technique has been applied to study a varied range of colloidal phenomena,<sup>[7]</sup> for instance nucleation and growth of colloidal crystals,<sup>[8,9]</sup> and shear-induced formation and melting of crystals.<sup>[10–12]</sup> Moreover, the further development of confocal microscopy has gained considerable momentum the last 10 years,

especially considering the resolution of this technique. Mostly using techniques which modify the response to a point light source of the microscope, also known as “point-spread-function engineering,” the resolution of fluorescence confocal microscopy has been increased well below 100 nm even in 3D.<sup>[13]</sup> An example of how the point-spread function can be modified is applied in stimulated emission depletion (STED) confocal microscopy. Already this technique has been demonstrated with spherical fluorescently labeled silica particles developed by procedures from our group.<sup>[14]</sup> Rod-like particles, however, occur far less frequently in colloidal microscopy studies. In fact, there are only a few anisotropic experimental systems that are suitable for confocal microscopy studies, e.g., poly(methyl methacrylate) (PMMA) ellipsoids obtained by stretching spheres, and dumbbell-shaped particles made from fluorescent core-shell particles of silica.<sup>[15–18]</sup> To this date, however, our silica rods are the only system that forms isotropic, nematic, and smectic phases and can be imaged quantitatively on the single particle level. Therefore, this system offers interesting new possibilities for real-space studies of anisotropic colloids.

As indicated before, the silica rods need to be labeled with a fluorescent dye in order to use them in fluorescence confocal microscopy studies. A method to label silica colloids with fluorescent dyes, such as rhodamine isothiocyanate (RITC) and fluorescein isothiocyanate (FITC), was developed by van Blaaderen and co-workers.<sup>[19,20]</sup> In this method, the dye molecules are chemically connected to a silane-coupling agent, (3-aminopropyl)triethoxysilane (APS), so that covalent bonding of the dye molecules to the silica-matrix is achieved, which gives the possibility to obtain homogeneously labeled spheres. Also, it is possible to obtain particles with (multiple) fluorescent shells when seeded growth is used. In this paper, we explored the method of van Blaaderen and co-workers in different ways to prepare three types of fluorescently labeled silica rods. The resulting particles each have their own characteristic fluorescent pattern. One of

Dr. A. Kuijk, Dr. A. Imhof, T. H. Besseling,  
Prof. A. van Blaaderen  
Soft Condensed Matter,  
Debye Institute for Nanomaterials Science  
Department of Physics and Astronomy  
Utrecht University  
Princetonplein 5, 3584 CC Utrecht, The Netherlands  
E-mail: A.Kuijk@uu.nl; A.vanBlaaderen@uu.nl

Dr. M. H. W. Verkuijlen, Dr. E. R. H. van Eck  
Institute for Molecules and Materials  
Radboud University  
Heyendaalseweg, 135, 6525 AJ Nijmegen, The Netherlands



DOI: 10.1002/ppsc.201300329

these patterns in particular, the gradient pattern, offers interesting new possibilities for future studies in which information on the directionality of the rods is important. The fluorescent rod-shaped particles are not only interesting for real-space studies as colloidal model system but also provide new opportunities for the many other uses of fluorescent particles, such as in barcoding applications.<sup>[21–23]</sup> Additionally, we will illustrate preliminary measurements on our FITC-labeled rods that STED microscopy also can be used without any modifications to the particles with significantly increased resolution.

## 2. Experimental Section

**Particle Preparation.** A detailed description of all syntheses including suppliers of chemicals and so on can be found in the Supporting Information.

Rods ( $R_{char}$ ) for NMR, adsorption, TGA measurements, and elemental analysis were prepared following the method described in Kuijk et al.<sup>[1]</sup> These rods had an end-to-end length  $L$  of 1.6  $\mu\text{m}$ , a diameter  $D$  of 310 nm, and polydispersities in these parameters of 15% and 20%, respectively.

Rods with a gradient in fluorescence level ( $R_{grad}$ ) were prepared by first bonding the dye (FITC or RITC) to a coupling agent (APS). Subsequently, the standard synthesis procedure was followed, adding the dye/APS mixture at the same time as the silica precursor [tetraethyl orthosilicate (TEOS)]. The rods had an average length  $L$  of 2.1  $\mu\text{m}$  and an average diameter  $D$  of 300 nm.

Rods with a uniform fluorescence level ( $R_{uni}$ ) were prepared using a mixture of 3.0 mL of TEOS and 35  $\mu\text{L}$  of APS instead of only TEOS. After synthesis, these rods were dispersed in a solution of dye in ethanol to let the dye diffuse into the rods and bond with the APS.

Rods into which two different dyes were incorporated ( $R_{2col}$ ) were grown in two reaction steps. In the first step of the synthesis, an RITC–APS reaction product was added together with the TEOS. After one night, TEOS and an FITC–APS reaction product in ethanol were added.

Rods ( $R_{shell}$ ) with a (45 nm) fluorescent shell around their nonfluorescent core ( $L = 3.2 \mu\text{m}$  and  $D = 320 \text{ nm}$ ) were prepared as described in Kuijk et al.<sup>[1]</sup> When RITC was used to label the shell, the rods were washed in a mixture of ethanol and ammonia (5 mL of ammonia per 100 mL of ethanol) to keep them stable. After the growth of an additional nonfluorescent shell of  $\approx 50 \text{ nm}$ , the rods were stable in ethanol. This extra layer was found to be necessary because RITC, being cationic under neutral conditions in water, compromises the stability of the otherwise negatively charged silica. Without the extra nonlabeled silica layer the rods aggregated.

Stöber silica spheres (St) were synthesized by the Stöber method.<sup>[3]</sup> These spheres had a diameter of 606 nm and a polydispersity of 10%. Silica spheres with APS built in ( $S_{dij}$ ) had a diameter of 225 nm and a polydispersity of 5%. These spheres were made fluorescent the same way as the  $R_{uni}$  rods.

**Particle Characterization.** The refractive index of the particles was measured using oils of varying refractive index (using steps of 0.01, Cargille refractive index liquids, measured at 589.3 nm at 25 °C).

The density of the particles was measured using a mixture of bromoform and methanol. Centrifugation at 700 g for 15 min showed whether rods in such a mixture creamed or sedimented. The composition of the mixture between creaming and sedimentation was converted to a density using figure 1 from Tolpekin et al.<sup>[24]</sup>

Thermogravimetric analysis (TGA) was performed in ambient air using a Pyris 1 machine of Perkin Elmer. The temperature was raised from 30 to 900 °C at rate of 10 °C  $\text{min}^{-1}$ . At 150 °C, a drying step of 30 min was inserted. The sample stayed at 900 °C for 1 min. Samples were prepared by centrifuging dispersions of silica particles in ethanol, removing the supernatant as much as possible, and drying the particles for one night at 50 °C.

$\text{N}_2$ -adsorption measurements were performed at  $-196 \text{ °C}$  using a Micromeritics Tristar 3000. Before the measurement, the particles were dried at 300 °C for 24 h.

Elemental analysis was performed by Mikroanalytisches Laboratorium Kolbe in Germany. For carbon (C), nitrogen (N), and hydrogen (H), combustion analysis was done using a CHNOS analyzer. Silicon (Si) was measured with inductively coupled plasma (ICP) analysis.

$^{29}\text{Si}$  solid-state nuclear magnetic resonance (NMR) experiments were performed on a 300 MHz/7.05 T Varian VNMR spectrometer using a 7.5-mm pencil-type MAS probe resonant at 59.596 MHz for silicon and 300.15 MHz for protons. Magic angle spinning at 5 kHz was employed. All spectra were recorded using spinal decoupling at 25 kHz RF field strength (pulse duration 20  $\mu\text{s}$  and 6° phase). For spin-lattice ( $T_1$ ) relaxation measurements, ramped cross polarization at a proton RF field strength of 25 kHz and a 29-kHz RF field on silicon was employed with an 8-ms contact time. The chemical shift was referenced with respect to tetramethylsilane (TMS) using the resonance of zeolite A at  $-89.7 \text{ ppm}$ .

Preliminary STED confocal images were taken with a Leica TCS SP5 equipped with continuous wave (CW)-gated STED. STED was performed with a CW excitation light source (solid-state laser at 592 nm wavelength), imaged in CW-STED mode was done using a pulsed excitation at 488 nm with a white light continuum laser. The 3D image stack was deconvolved with commercially available software (Huygens Professional STED module, Scientific Volume Imaging) using a theoretical point spread function.

## 3. Results and Discussion

### 3.1. Material Properties

Spherical silica particles have been used as a popular model system in colloid science since Stöber et al.<sup>[3]</sup> reported their synthesis of monodisperse spherical colloids in 1968. As the method that we developed to grow the silica rods also uses base-catalyzed hydrolysis and condensation of alkoxy silanes, we compared the material properties of this so-called Stöber silica (St) with those of silica rods made following the procedure from Kuijk et al.<sup>[1]</sup> ( $R_{char}$ ).

Properties that are of direct interest for use in confocal microscopy studies are the index of refraction and density.

**Table 1.** Density ( $\rho$ ) and refractive index ( $n$  at  $\lambda = 589.3$  nm,  $T = 25$  °C) of several systems of rods and Stöber silica spheres.

System	$L$ [ $\mu\text{m}$ ]	$D$ [nm]	$L/D$	$\rho$ [ $\text{g mL}^{-1}$ ]	$n$
B17	0.76	407	1.8	$1.90 \pm 0.04$	
B11	1.1	270	4.1	$1.90 \pm 0.03$	$1.455 \pm 0.005$
B22	1.6	335	4.8	$1.89 \pm 0.03$	
B23	2.1	252	8.4	$1.89 \pm 0.02$	$1.445 \pm 0.005$
St	–	606	1	$1.99 \pm 0.01$	$1.445 \pm 0.005$

**Table 1** shows that the index of refraction of the rods does not differ significantly from that of Stöber silica: both are close to 1.45. The density, however, is slightly lower for the rods, which suggests that they have a more porous structure and that these pores are accessible for the liquid the rods are dispersed in.

More information about the porosity of the structure was obtained by  $\text{N}_2$ -adsorption measurements of particles first dried at 300 °C, at which all physically adsorbed water is evaporated from the particles' pores. The results showed that the BET (Brunauer–Emmett–Teller)-surface area of the spheres was much smaller ( $6.1 \text{ m}^2 \text{ g}^{-1}$ ) than that of the rods ( $47.7 \text{ m}^2 \text{ g}^{-1}$ ). The actual geometrical surface areas of the spheres and rods are  $5.0 \text{ m}^2 \text{ g}^{-1}$  and  $8.0 \text{ m}^2 \text{ g}^{-1}$ , respectively. This means that 18% of the measured BET-surface area of the Stöber spheres stems from internal pores, while this value is 83% for the rods. Here, we assumed that the surface roughness was the same for both particles as was indeed the case as observed in transmission electron microscopy (see Supporting Information). The rods thus have a more porous structure than the spheres. This was confirmed by the determination of pore volumes for pore diameters between 1 and 300 nm: a significantly larger pore-volume was measured for the rods ( $0.034 \pm 0.003$  vs  $0.013 \pm 0.001 \text{ cm}^3 \text{ g}^{-1}$ ).

The higher porosity of the rods compared with Stöber silica can be explained by the presence of polyvinylpyrrolidone (PVP) in the structure. PVP is a polymer that adsorbs onto silica and is used in the synthesis of the rods but not in that of the spheres. This hypothesis is supported by the observation that the rods looked brownish white after heating to 300 °C for the  $\text{N}_2$ -adsorption measurement, which indicates that something was pyrolyzed: probably PVP. TGA confirmed this observation; the rods decreased more in weight than the Stöber silica: 12% versus 7% (**Figure 1b**). The temperature of around 400 °C at which the additional 5% decrease for rods occurs is the temperature at which PVP gets oxidized (see Zheng et al.<sup>[25]</sup>).

Elemental analysis and  $^{13}\text{C}$  CPMAS solid-state NMR were used to obtain more direct proof of the presence of PVP inside the rods. Elemental analysis was done for carbon, hydrogen, nitrogen, and silicon. The results are listed in **Table 2**. The presence of N atoms in the rods is an indication for PVP molecules, which is the only species in the

**Table 2.** Elemental analysis results in weight percentages.

System	C [%]	H [%]	N [%]	Si [%]
Rods ( $R_{char}$ )	3.48	1.20	0.68	38.96
Spheres (St)	1.12	0.91	0.01	44.08

synthesis that contains nitrogen apart from the (gaseous) catalyst ammonia. From the measurements for Stöber silica, we know that ammonia does not stay inside the silica structure, as there were no N atoms detected for the spheres. The total weight percentage of PVP calculated from the elemental analysis results is 5.4%, which corresponds well to the value of 5% found in the TGA measurement. Ethoxy signals were confirmed in the  $^{13}\text{C}$  CPMAS NMR measurements of the Stöber spheres and were next to PVP signals present in the NMR spectra of the rods as well (see Supporting Information). Because the elemental analysis and thermogravimetry had already given quantitative results that agreed well, the NMR results were not made quantitative by performing direct  $^{13}\text{C}$  NMR experiments. The amount of PVP per unit surface can be calculated using the elemental analysis data. Assuming all PVP is adsorbed on the geometrical surface of the rods, we found an amount of  $7.4 \text{ mg m}^{-2}$ . Compared with the maximum adsorption of  $0.8 \text{ mg m}^{-2}$  for PVP25 (molecular weight:  $25\,000 \text{ g mol}^{-1}$ ) on silica that was found by van der Beek and Cohen Stuart,<sup>[26]</sup> this seems to be too high. It is therefore more likely that the PVP was also built in the internal structure of the rods, causing the higher porosity. If we assume that the density of PVP inside the rods was around  $1 \text{ g cm}^{-3}$ , the internal volume was on the order of 5%, if we assume half of the PVP was present inside the particles and half was on the outside. This conservative estimate is on the same order as the internal pore volume found with the  $\text{N}_2$ -adsorption measurements, which makes it likely that all PVP was already burned away at 300 °C.

The water content of the rods was measured in drying steps before the TGA and elemental analysis (**Figure 1a**). The rods were dried at 150 °C for 30 min for the TGA measurements and at 100 °C for one night for the elemental analysis. After drying, the rods had lost on average 8.7% of their weight and

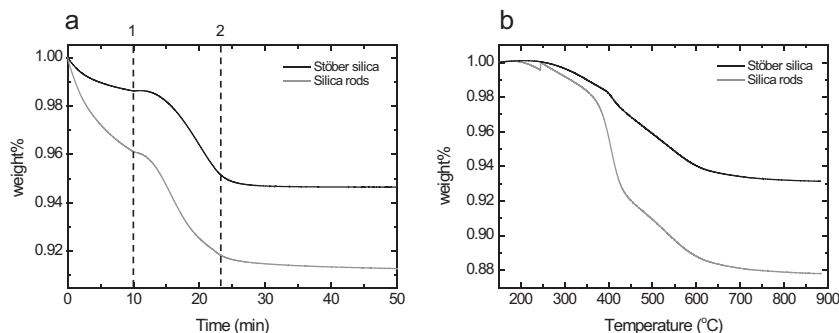
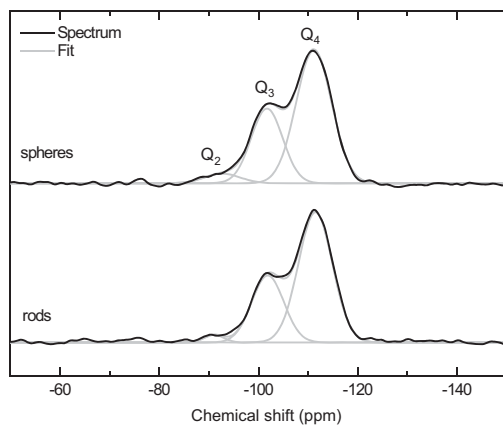


**Figure 1.** Thermogravimetric analysis (TGA) of silica rods ( $R_{char}$ ) and spheres (St). a) Drying step before TGA measurement; the Stöber silica spheres contain less water than the silica rods. (1: heating from 30 to 150 °C, 2: constant temperature of 150 °C). b) TGA measurement after drying step. The temperature was increased with 10 °C per min. The rods lose more weight than the spheres.



System	Site	Chem. shift (ppm)	$T_1$ (s)	$A_R$
spheres (St)	Q <sub>2</sub>	-92.7	168	0.9%
	Q <sub>3</sub>	-101.7	81 (52%)	30.2%
	Q <sub>4</sub>	-111.2	504 (48%)	68.9%
rods ( $R_{char}$ )	Q <sub>2</sub>	-91.0	181	1.4%
	Q <sub>3</sub>	-101.9	199	28.3%
	Q <sub>4</sub>	-111.5	400	70.4%

**Figure 2.**  $^{29}\text{Si}$  solid-state NMR spectra (black) of silica rods ( $R_{char}$ ) and Stöber silica spheres (St). Exact positions and relative areas were determined by fitting Gaussian functions (gray) to the spectra. The table below the spectra shows the positions,  $^{29}\text{Si}$  spin lattice relaxation times ( $T_1$ ), and relative areas ( $A_R$ ) of the peaks. The accuracy in the relative areas is estimated at  $\pm 1\%$ .

the spheres 4.7%. The rods thus contained more water than the spherical colloids, as was expected from the higher porosity of the rods.

Although the physical structure of the rods is more porous than that of the spheres, their chemical structure with respect to the number of silicon atoms which is bonded to other silicon atoms through an oxygen atom is more or less similar within error. Using direct excitation  $^{29}\text{Si}$  solid-state NMR, the atomic surrounding of the silicon atoms in the structure was quantitatively determined. The resulting spectra are shown in **Figure 2**. The three peaks in these spectra correspond to silicon atoms that are bound to other silicon atoms through 4 (Q<sub>4</sub>), 3 (Q<sub>3</sub>) or 2 (Q<sub>2</sub>) Si–O–Si bonds. The other groups around the silicon atom are ethoxy or hydroxy groups. Quantitative  $^{29}\text{Si}$  solid-state NMR measurements showed that the silica which the rods and spheres are made of both consist of about 69% of Q<sub>4</sub>, 29% of Q<sub>3</sub>, and around 1% of Q<sub>2</sub>, which is consistent with earlier measurements for colloidal Stöber silica.<sup>[27,28]</sup>

### 3.2. Fluorescent Labeling

In order to use silica rods as model particles in confocal fluorescence microscopy studies, fluorescent labeling is essential. To covalently bind fluorescent dye molecules to the silica-matrix, a silane-coupling agent was used (similarly to the method reported for fluorescent silica spheres).<sup>[19,20]</sup> Depending on how this technique was implemented in the rod synthesis, three different fluorescent patterns resulted. **Figure 3** shows these three patterns: rods with a gradient in fluorescence from head to tail ( $R_{grad}$ ), rods with a constant fluorescence level ( $R_{uni}$ ), and rods

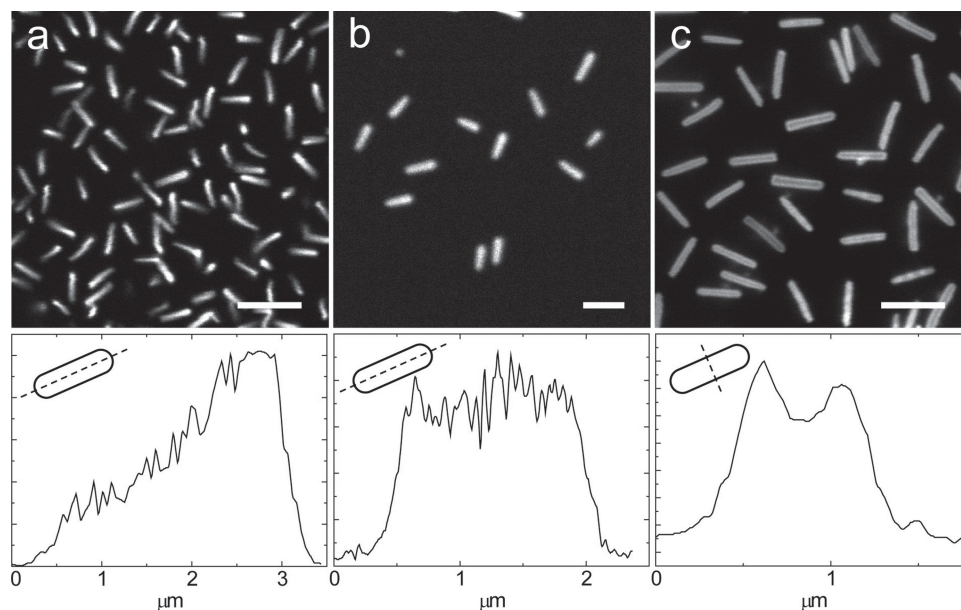


**Figure 3.** Rods with different fluorescent patterns in confocal images and corresponding graphs of intensity as a function of position in a rod. a) System  $R_{grad}$ : decreasing fluorescence toward the tail in rods when APS/dye complexes were added at the start of rod growth. b) System  $R_{uni}$ : homogeneously labeled rods when APS was built in during synthesis and FITC or RITC were added afterward. c) System  $R_{shell}$ : 30-nm thick fluorescent silica shells around a nonfluorescent core of the same diameter ( $\approx 300$  nm) as the rods in a) and b). Scale bars indicate 5  $\mu\text{m}$  for a) and c), and 2  $\mu\text{m}$  for b).

**Table 3.** Summary of the results of the described labeling methods.

Fluorescent pattern	(Dis)advantages of the method
Gradient (APS/dye added from start)	+ Distinction between two ends
	– Gradient makes confocal images harder to quantify
Homogeneous (APS added from start)	+ Most easy to find orientations and positions
	– Low fluorescence intensity
Shell (APS/dye added after growth)	+ Most control over rod dimensions
	– Aggregation during shell formation

with a fluorescent shell ( $R_{shell}$ ). The advantages and drawbacks of the different labeling methods, as described in detail below, are compared in **Table 3**.

When the dye was covalently bound to the coupling agent (APS) before addition to the synthesis mixture, particles with a dye-concentration decreasing from head to tail were formed (Figure 3a). An explanation for this phenomenon is offered by the growth mechanism of the rods.<sup>[1]</sup> Summarized, a silica nucleus is formed at the interface of polymer-rich emulsion droplets of water in pentanol. Hydrolyzed TEOS molecules get dissolved in the emulsion droplet and grow onto the nucleus from the droplet-side only. There is an intriguing mechanistic overlap with the growth of silica shells on nanoparticles that are dispersed in the water droplets of a water in oil microemulsion. It was found by some of us that, depending on the polarity of the nanoparticle surface coating (and thus whether the nanoparticle was at the edge of the water droplet or right in the middle), the nanoparticle ended up straight in the middle of the silica or at the edge.<sup>[29]</sup> When APS/dye-reaction products are added to the synthesis mixture, they dissolve most likely directly in the emulsion droplets without hydrolysis of the APS units because of the more polar character of the dye molecules and the more polar amine group. TEOS, however, dissolves better in the continuous pentanol phase, and dissolves into water only after being hydrolyzed, which is a relatively slow process. So, while there is a more or less constant feed of TEOS, the availability of dye is high at the start and decreases during growth, resulting in a concentration gradient of built-in dye molecules over the length of the rod. Attempts to replenish the available APS/dye-reaction products during rod growth did not result in a more constant level of fluorescence. APS/dye-reaction products that were added later during the synthesis did not dissolve in the emulsion droplets, but grew mostly on the outer surface of the entire rod. This is shown clearly in **Figure 4**, where two different dyes were used: one for the initial addition (FITC) and another for the addition after 1 d (RITC). The preferential growth on the outside of the rod was already noticeable when APS/dye-reaction products were

added 1 h after the addition of TEOS instead of directly after TEOS addition. A probable explanation for the fact that dye attached to the coupling agent did not reach the water droplet when added later is that (partially) hydrolyzed TEOS molecules reacted with it and the outer silica before it was able to reach the water. Further research needs to take place to further test this hypothesis. Long rods, for which a two-step synthesis with TEOS is required, are best grown by adding only TEOS in the second step and no extra dye, to prevent the formation of a fluorescent shell.

An interesting feature of the rods with a gradient in fluorescence is the possibility provided to distinguish between the round and the flat end of the rod. The same holds for the rods that were labeled with two different dyes shown in **Figure 4a**. Using the particles with a gradient pattern, we examined the influence of the flat end on the orientation of the rods in a smectic phase. **Figure 5** shows an SEM and a confocal image of rods in such a phase. From both images, we can conclude that the orientation of neighboring rods is random; the fraction of neighboring rods that point in the same direction is roughly equal to the fraction that points in opposite directions. The rods thus behave as if they have symmetric ends, at least with respect to their ordering in the liquid crystal phases observed with them so far. A second example of an experimental application of the  $R_{grad}$  rods is shown in **Figure 5c,d**. While the rods in dilute dispersions are randomly oriented, they align when an electric field is applied.<sup>[30]</sup> From theory, it is known that the shape of the particle matters for the alignment in electric fields.<sup>[31]</sup> Since the ends of our rods are not identical in shape, it would therefore be interesting to investigate the influence of this anisotropy on the alignment. **Figure 5c** shows that no preferred directional alignment was visible when the rods were placed in an  $0.02 \text{ V } \mu\text{m}^{-1}$  DC field. This is even clearer when a  $0.25 \text{ V } \mu\text{m}^{-1}$ , 1-MHz AC field was applied in addition to the DC field (**Figure 5d**), which aligned the particles such that they oriented parallel to the field direction, with still no preference for directing left or right. It is important to point out here that we recently found that the combination of a geometrical difference of the two ends of our rods and a likely chemical difference in the surface tension on the two ends is sufficient to direct the growth of polymethylmethacrylate and polystyrene specifically only at the flat and of the particles.<sup>[32]</sup>

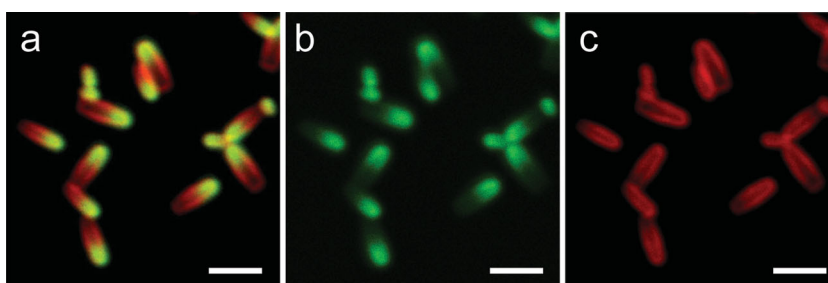


**Figure 4.** Rods with two different fluorescent dyes built in ( $S_{2col}$ ). a) FITC and RITC signal combined in one image. b) FITC signal only. FITC was added directly at the start of the synthesis. Fluorescence was mainly measured in the first half of the rods that had grown during the first day. c) RITC signal only. RITC (and TEOS) was added after 1 d and was incorporated in shells around the already existing particle and the additionally grown second half of the rod. Scale bars indicate  $2 \mu\text{m}$ .

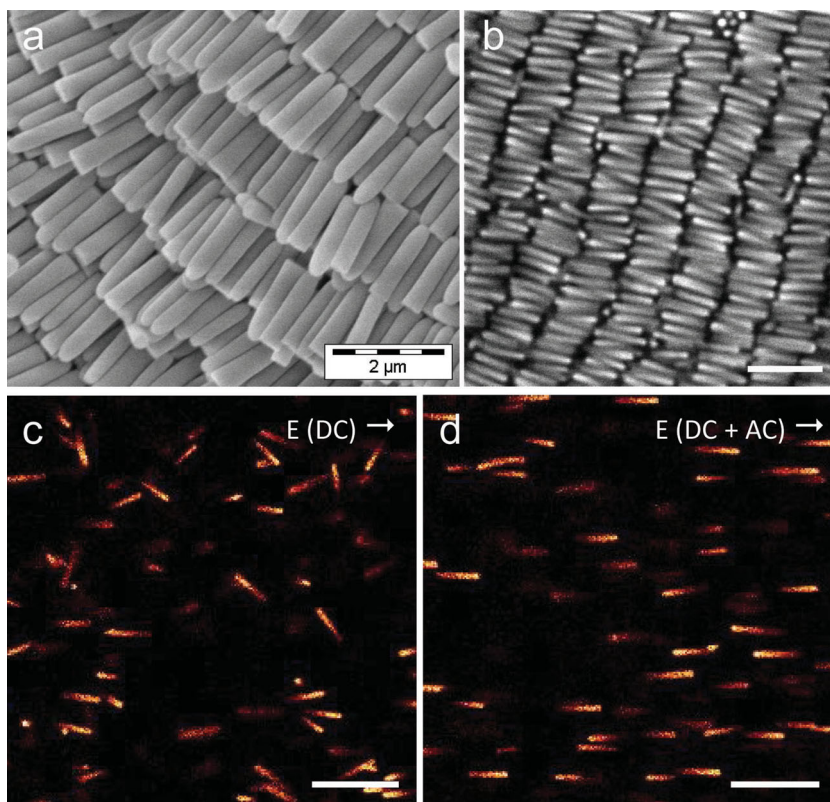


**Figure 5.** Examples of experimental applications of  $R_{grad}$  rods. a) Scanning electron microscopy (SEM) image of rods in a smectic or crystal phase. b) Confocal microscopy image of  $R_{grad}$  rods in a smectic liquid crystal phase. Scale bar indicates  $5 \mu\text{m}$ . Both a) and b) images show that the orientation of the rods within the layers is random. c) Rods pointing in random directions when a  $0.02 \text{ V } \mu\text{m}^{-1}$  DC field was applied to a dilute isotropic phase. d) The same system as in c), with the addition of a  $0.25 \text{ V } \mu\text{m}^{-1}$ ,  $1 \text{ MHz}$  AC field. The rods aligned, but orientation to the left or the right was random. Scale bars indicate  $10 \mu\text{m}$ .

Instead of letting APS and dye react before addition to the rod synthesis, it turned out to be also possible to bind the dye to the APS after incorporation of APS in the rods. Unlike APS that was coupled to a dye, uncoupled APS was apparently built in more homogeneously throughout the rods (Figure 3b). From this, we conclude that the dye molecule, when chemically coupled to APS, caused the gradient pattern described in the previous section and not the APS molecule by itself. In case uncoupled APS was added to the synthesis mixture, APS and TEOS both acted as silica precursor and the resulting particles consisted of a silica-matrix with more homogeneously distributed  $-\text{C}_3\text{H}_6\text{NH}_2$  groups. The pores of the rods were sufficiently large to make the rods fluorescent by letting RITC or FITC molecules diffuse into the structure and bind to the free  $-\text{C}_3\text{H}_6\text{NH}_2$  groups, despite the presence of PVP molecules. The resulting rods had a homogeneous distribution of incorporated fluorescent dye molecules, at least as far as can be observed within the limits of confocal resolution (Figure 3b). The intensity of the fluorescence, however, was lower than that of the rods with a gradient in fluorescence (Figure 6). Rods in which no APS was incorporated also showed a weak fluorescence signal after dye molecules were allowed to diffuse into them, but this signal was even weaker because most dye molecules were washed out during the washing steps to remove

the dye from the solvent. This was not the case for dye molecules that were covalently bound to the silica-matrix. The method of incorporating APS first and subsequently letting dye diffuse in the particles also worked for Stöber silica spheres, but less well, since these particles are less porous as indicated by the BET-surface area results and also described in the literature<sup>[33]</sup> (Figure 6). It should be remarked though, that we did not quantify yet how much of the APS was built into the rods (as compared with how much was built into the spheres<sup>[28]</sup>).

The third way of labeling the rods is the growth of a fluorescently labeled shell after preparation of nonfluorescent rod cores. Figure 3c shows rods with a  $30 \text{ nm}$  shell of fluorescently labeled silica around their  $300 \text{ nm}$  nonfluorescent cores. The method of coating silica rods with a fluorescent shell is in this case analogous to the coating of spheres. Unfortunately, the problem of aggregation was much more pronounced for the coating of rods. In the literature, aggregation is attributed to the presence of APS molecules on the surface of the silica particles.<sup>[28,34,35]</sup> These decrease the stabilizing negative surface charge of the silica layer by its basic amino groups, resulting in less stable particles. Aggregation could be reduced by decreasing the ammonia concentration or by dilution of the core suspension during shell growth. Additionally, aggregates were removed from the sample by repeated sedimentation after which only the particles in the top part of the supernatant were used. We noticed that

aggregation was much more severe when RITC was used compared with FITC. Both RITC-coated rods and RITC-labeled

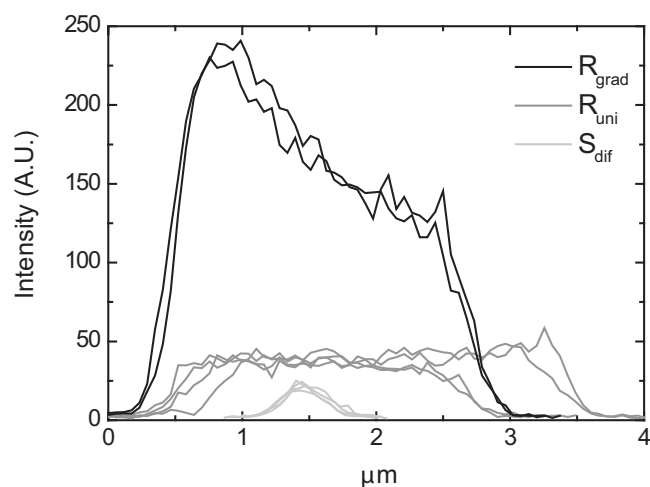


**Figure 6.** Comparison of intensities of fluorescence along the long axis of a number of rods with dye built directly ( $R_{grad}$ ), rods with dye diffused in ( $R_{uni}$ ), and spheres with dye diffused ( $S_{dif}$ ). All spectra were recorded with equal settings.

spheres were not stable in pure ethanol. The addition of ammonia to unstable dispersions in ethanol restored colloidal stability, when the final concentration was higher than 0.5 M. An explanation for this observation is also offered by charge stabilization. The FITC molecule is negatively charged in ethanol, because part of its hydroxyl groups are dissociated, and therefore enhances the negative surface charge of silica. RITC, on the other hand, is also a base counteracting the negative surface charge. Additionally, the basic amino groups of unbound APS reduce the surface charge of the particles, which causes aggregation. It is likely that the addition of ammonia cancels this effect because it induces dissociation of the carboxyl group by increasing the pH. After the growth of an additional non-fluorescent shell, the RITC-labeled particles were found to be stable in pure ethanol again. The fact that aggregation did not occur in the rod synthesis when unbound APS or the APS/dye-reaction product was added is probably due to PVP that acts as a steric stabilizer on the surface of the rods.

To demonstrate that fluorescently labeled silica rods cannot only be used in normal microscopy but are also suitable for high-resolution techniques such as STED confocal microscopy, we performed some preliminary measurements shown in Figure 7. Figure 7a shows a 2D slice out of a 3D data set that was taken of a sample of  $R_{shell}$  rods in an index matching DMSO/water mixture after sedimentation, at a packing fraction above 50%. Figure 7b clearly shows the increased resolution when the same particles were imaged in CW-STED mode using a pulsed excitation at 488 nm with a white light continuum laser. As a result of the improved resolution, the fact that the FITC is localized in a very thin (30 nm) shell is much better visible, especially for rods oriented perpendicularly to the imaging plane. The resolution can be even further increased by

3D STED deconvolution (Figure 7c), thereby also significantly reducing background noise.

#### 4. Conclusions

The material properties of colloidal silica rods were compared with those of Stöber silica spheres. It was found that the refractive index of rods and spheres is equal ( $1.450 \pm 0.005$ ), while the density of rods is slightly lower than that of spheres ( $1.90$  vs  $1.99 \text{ g cm}^{-3}$ ). Furthermore, the porosity of the rods was higher than that of the spheres. Elemental analysis showed that this is most likely caused by the presence of about 5% by weight of PVP molecules inside the silica-matrix of the rods. Despite their more open structure, the chemical structure of the silica that the rods and spheres consist of was equal within error. They consist of a not fully condensed siloxane structure, of which 69% is  $Q_4$ , 39% is  $Q_3$ , and around 1% is  $Q_2$ .

In order to study the system with confocal fluorescence microscopy, silica rods were labeled with a fluorescent dye using three different methods, which resulted in different fluorescence patterns (see Table 3). Due to their asymmetric growth-mechanism, rods were created with a decreasing gradient in concentration from head to tail. These rods make it possible to distinguish between the rods' round head and flat tail. A homogeneous distribution of dye molecules was achieved by the incorporation of APS molecules that were subsequently bound to dye molecules that diffused into the rods. The fluorescence intensity of these rods, however, was low. Finally, fluorescent shells were grown successfully after rod growth was finished in an ethanol/water/ammonia mixture, similarly to shell growth around silica spheres. Combining these methods using different dyes, as was already demonstrated by using just two dyes, makes the synthesis of fluorescent silica rods not only very interesting for studies in which the rods are used as (soft) condensed matter model studies but also provide new possibilities for the many other uses that fluorescent silica spheres have already been used for such as barcoding, biological labeling and sensing, and nanomedicine.

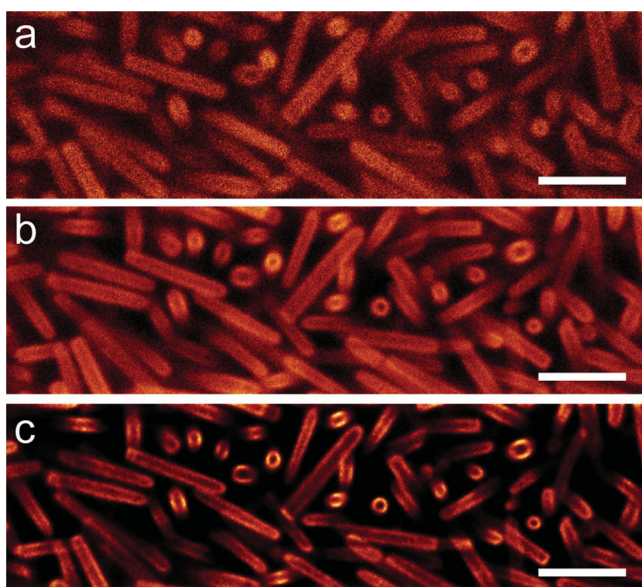


**Figure 7.** Difference between a) conventional confocal microscopy, and b) STED confocal microscopy. In b), the location of the dye in the outer shell is much better visible due to the increased resolution. c) Further improvement of the resolution by 3D STED deconvolution. Scale bars indicate 3  $\mu\text{m}$ .

#### Supporting Information

Details on the synthesis procedures and  $^{13}\text{C}$  CPMAS solid-state NMR measurements are described in the Supporting Information. Supporting Information is available from the Wiley Online Library or from the author.

#### Acknowledgements

Arno Kentgens (Radboud University, Nijmegen, the Netherlands) is acknowledged for helpful discussions regarding the solid-state NMR measurements. Furthermore, the authors acknowledge the Netherlands Organization for Scientific Research (NWO) for their support of the solid-state NMR facility for advanced materials research. Leica is acknowledged for allowing the authors to perform test measurements on their SP5 system. The authors thank Marjan Versluijs-Helder and Tamara Eggenhuisen from the Department of Inorganic Chemistry and Catalysis of Utrecht University for performing the TGA and  $\text{N}_2$ -adsorption measurements. This research was carried out partially (THB) under project number M62.7.08SDMP25 in the framework of the

Industrial Partnership Program on Size Dependent Material Properties of the Materials innovation institute (M2i) and the Foundation of Fundamental Research on Matter (FOM), which is part of the Netherlands Organisation for Scientific Research (NWO).

Received: October 12, 2013

Revised: November 28, 2013

Published online: February 11, 2014

- 
- [1] A. Kuijk, A. van Blaaderen, A. Imhof, *J. Am. Chem. Soc.* **2011**, *133*, 2346.
- [2] A. Kuijk, D. V. Byelov, A. V. Petukhov, A. van Blaaderen, A. Imhof, *Faraday Discuss.* **2012**, *159*, 181.
- [3] W. Stöber, A. Fink, E. Bohn, *J. Colloid Interface Sci.* **1968**, *26*, 62.
- [4] R. Besseling, I. Lucio, E. R. Weeks, W. C. K. Poon, *Adv. Colloid Interface* **2009**, *146*, 1.
- [5] A. van Blaaderen, *Prog. Colloid Polym. Sci.* **1997**, *104*, 59.
- [6] A. D. Dinsmore, E. R. Weeks, V. Prasad, A. C. Levitt, D. A. Weitz, *Appl. Optics* **2001**, *40*, 4152.
- [7] V. Prasad, D. Semwogerere, E. R. Weeks, *J. Phys.: Condens. Matter* **2007**, *19*, 113102.
- [8] U. Gasser, E. R. Weeks, A. Schofield, P. N. Pusey, D. A. Weitz, *Science* **2001**, *292*, 258.
- [9] J. P. Hoogenboom, P. Vergeer, A. van Blaaderen, *J. Chem. Phys.* **2003**, *119*, 3371.
- [10] Y. L. Wu, D. Derks, A. van Blaaderen, A. Imhof, *Proc. Natl. Acad. Sci.* **2009**, *106*, 10564.
- [11] D. Derks, Y. L. Wu, A. van Blaaderen, A. Imhof, *Soft Matter* **2009**, *5*, 1060.
- [12] T. H. Besseling, M. Hermes, A. Fortini, M. Dijkstra, A. Imhof, A. van Blaaderen, *Soft Matter* **2012**, *8*, 6931.
- [13] S. Hell, *Nat. Methods* **2009**, *6*, 24.
- [14] K. I. Willig, J. Keller, M. Bossi, S. W. Hell, *New J. Phys.* **2006**, *8*, 106.
- [15] A. Mohraz, M. J. Solomon, *Langmuir* **2005**, *21*, 5298.
- [16] D. Mukhija, M. J. Solomon, *Soft Matter* **2011**, *7*, 540.
- [17] P. M. Johnson, C. M. van Kats, A. van Blaaderen, *Langmuir* **2005**, *21*, 11510.
- [18] A. F. Demirors, P. M. Johnson, C. M. van Kats, A. van Blaaderen, A. Imhof, *Langmuir* **2010**, *26*, 14466.
- [19] A. van Blaaderen, A. Vrij, *Langmuir* **1992**, *8*, 2921.
- [20] N. A. M. Verhaegh, A. van Blaaderen, *Langmuir* **1994**, *10*, 1427.
- [21] L. Grondahl, B. J. Battersby, D. Bryant, M. Trau, *Langmuir* **2000**, *16*, 9709.
- [22] L. Xia, T. Q. Wang, J. H. Zhang, D. F. Zhu, X. Zhang, Y. Ning, H. Zhang, B. Yang, *ACS Nano* **2010**, *4*, 4350.
- [23] A. Schulz, C. McDonagh, *Soft Matter* **2012**, *8*, 2579.
- [24] V. A. Tolpekin, M. H. G. Duits, D. van den Ende, J. Mellema, *Langmuir* **2004**, *20*, 2614.
- [25] M. P. Zheng, Y. P. Jin, L. G. Jin, M. Y. Gu, *J. Mater. Sci. Lett.* **2000**, *19*, 433.
- [26] G. P. van der Beek, M. A. Cohen Stuart, *Langmuir* **1991**, *7*, 327.
- [27] A. van Blaaderen, A. P. M. Kentgens, *J. Non-Cryst. Solids* **1992**, *149*, 161.
- [28] A. van Blaaderen, A. Vrij, *J. Colloid Interface Sci.* **1993**, *156*, 1.
- [29] R. Koole, M. M. van Schooneveld, J. Hilhorst, C. de Mello Donegá, D. C. 't Hart, A. van Blaaderen, D. Vanmaekelbergh, A. Meijerink, *Chem. Mat.* **2008**, *20*, 2503.
- [30] A. Kuijk, T. Troppenz, L. Fillion, A. Imhof, R. van Roij, M. Dijkstra, A. van Blaaderen, unpublished.
- [31] B. W. Kwaadgras, M. Dijkstra, R. van Roij, *J. Chem. Phys.* **2012**, *136*, 131102.
- [32] B. Peng, M. Kamp, J. D. Meeldijk, B. de Nijs, A. van Blaaderen, A. Imhof, unpublished.
- [33] A. Labrosse, A. Burneau, *J. Non-Cryst. Solids* **1997**, *221*, 107.
- [34] C. Vonk, S. M. Oversteegen, J. E. G. J. Wijnhoven, *J. Colloid Interface Sci.* **2005**, *287*, 521.
- [35] A. Imhof, M. Megens, J. J. Engelberts, D. T. N. de Lang, R. Sprik, W. L. Vos, *J. Phys. Chem. B* **1999**, *103*, 1408.
-